PAPER • **OPEN ACCESS**

Assessing the quality of large-area monolayer graphene grown on liquid copper for size-selective ionic/molecular membrane separations

To cite this article: Grzegorz Romaniak *et al* 2023 *Mater. Res. Express* **10** 105101

Materials Research Express

PAPER

Assessing the quality of large-area monolayer graphene grown on liquid copper for size-selective ionic/molecular membrane separations

Grzegorz Romaniak[1], **Peifu Cheng**[2], **Konrad Dybowski**[1], **Piotr Kula**[1] and **Piran R Kidambi**[2,3,4,*]

[1] Faculty of Mechanical Engineering, Institute of Materials Science and Engineering, Lodz University of Technology, 1/15 Stefanowskiego St., 90-924 Lodz, Poland
[2] Department of Chemical and Biomolecular Engineering, Vanderbilt University, Nashville, Tennessee TN 37212, United States of America
[3] Department of Mechanical Engineering, Vanderbilt University, Nashville, Tennessee TN 37212, United States of America
[4] Vanderbilt Institute of Nanoscale Sciences and Engineering, Vanderbilt University, Nashville, Tennessee TN 37212, United States of America
[*] Author to whom any correspondence should be addressed.

E-mail: piran.kidambi@vanderbilt.edu

Keywords: atomically thin membranes, graphene, graphene membranes, molecular sieving, desalination, liquid copper growth, ionic/molecular separations

OPEN ACCESS

RECEIVED
26 March 2023

REVISED
19 July 2023

ACCEPTED FOR PUBLICATION
10 August 2023

PUBLISHED
12 October 2023

Abstract

Monolayer graphene growth on liquid copper (Cu) has attracted attention due to advantages of a flat/smooth catalytic growth surface, high synthesis temperature (>1080 °C) as well as the possibility of forming graphene domains that are mobile on the liquid Cu with potential to minimize grain boundary defects and self-assemble into a continuous monolayer film. However, the quality of monolayer graphene grown on liquid copper and its suitability for size-selective ionic/molecular membrane separations has not been evaluated/studied. Here, we probe the quality of monolayer graphene grown on liquid Cu (via a metallurgical process, HSMG®) using Scanning Electron Microscope (SEM), High-resolution transmission electron microscope (HR-TEM), Raman spectroscopy and report on a facile approach to assess intrinsic sub-nanometer to nanometer-scale defects over centimeter-scale areas. We demonstrate high transfer yields of monolayer graphene (>93% coverage) from the growth substrate to polyimide track etched membrane (PITEM, pore diameter ~200 nm) supports to form centimeter-scale atomically thin membranes. Next, we use pressure-driven transport of ethanol to probe defects > 60 nm and diffusion-driven transport of analytes (KCl ~0.66 nm, L-Tryptophan ~0.7–0.9 nm, Vitamin B12 ~1–1.5 nm and Lysozyme ~3.8–4 nm) to probe nanoscale and sub-nanometer scale defects. Diffusive transport confirms the presence of intrinsic sub-nanometer to nanometer scale defects in monolayer graphene grown on liquid Cu are no less than that in high-quality graphene synthesized via chemical vapor deposition (CVD) on solid Cu. Our work not only benchmarks quality of graphene grown on liquid copper for membrane applications but also provides fundamental insights into the origin of intrinsic defects in large-area graphene synthesized via bottom-up processes for membrane applications.

1. Introduction

Atomically thin 2D materials such as monolayer graphene presents potential for advancing membrane separations including nanofiltration [1, 2], desalination [3–5], ionic/molecular separation [5–8], proton transport [9–12], rapid water vapor transport [9], aerosol filtration [13], gas separation [14–16], DNA translocation [17, 18], dialysis [6, 7, 12, 19–22] and protein desalting [6, 19] among others, by simultaneously allowing very high permeance and extremely high selectivity. The realization of such advances, however, hinges on scalable synthesis of high-quality monolayer graphene and facile interfacing to enable practical membrane

separation applications [12, 19, 22]. Notably, membrane applications require significantly large areas and present different quality requirements than electronic applications [23]. For example, a few nanoscale vacancy defects can completely compromise membrane applications via non-selective leakage [5], but would barely be noticeable in most electronic device applications. Assessing the quality of monolayer graphene over large-area is hence imperative for enabling atomically thin membrane applications. However, probing sub-nanometer and nanometer scale defects over large-area required for membrane applications remains non-trivial [23, 24]. Conventional characterization techniques such as Raman spectroscopy are unable to resolve/detect an extremely low density or individual nanoscale or sub-nanometer scale defects, while scanning transmission electron microscopy (STEM) or scanning tunneling microscopy (STM) can probe individual nanoscale and sub-nanometer scale defects but are limited to small areas (probing centimeter-scale areas is prohibitively expensive in cost and time) [23, 24].

In this context, the synthesis of graphene on liquid copper via the metallurgical method (High Strength Metallurgical Graphene - HSMG®) has attracted attention as a new avenue for the scalable production of high-quality graphene [25–28] due to advantages such as: (*i*) it allows large graphene domains via low graphene nucleation density and faster growth rates at high temperature >1080 °C [29–35], (*ii*) the smooth liquid surface during growth coupled with the high temperature allows for potentially reduced defects in the graphene domains [29], and (*iii*) the liquid Cu enables the graphene domains to be mobile allowing self-assembly in a continuous film via domain rotation that could potentially minimize grain boundary defects [31, 36]. However, to the best of our knowledge, the quality of HSMG® for membrane applications (centimeter-scale areas) has not yet been assessed, evaluated or studied.

Here, we report on a facile approach to characterize quality of large-area HSMG® by forming atomically thin membranes and probing pressure-driven as well as diffusion-driven transport of analytes through the same membrane area. We probe sub-nanometer and nanometer scale defects over centimeter-scale areas of HSMG® and compare its quality with high-quality CVD graphene grown on solid Cu. Our results show that although liquid Cu method offers large graphene domains and potentially results in low-angle domain boundaries, intrinsic sub-nanometer and nanometer scale defects still exist and are no less than found in high-quality CVD graphene grown on solid Cu [5–7, 9, 10, 12, 13, 19–22, 24, 37]. Our results indicate that the quality of graphene for membrane applications and ionic/molecular transport in particular are susceptible to intrinsic defects incorporating within individual graphene domains during growth of monolayer graphene via bottom-up synthesis methods.

2. Materials and methods

2.1. Graphene growth

High Strength Metallurgical Graphene was synthesized on a liquid Cu surface as reported in detail elsewhere [35, 38, 39] with some minor modifications. At first, 0.2 mm Ni carburized foil was electroplated with Cu using a solution of copper sulphate pentahydrate ($CuSO_4{\cdot}5H_2O$), at a current density of 0.02 A cm^{-2}, for 6 h. Next, the plated foil was heated to 1060 °C under 10 Pa pressure in a reactor (SuperCarb, Seco/Warwick SA) and carburized in an atmosphere of acetylene (0.4 l min^{-1}), ethylene (0.4 l min^{-1}), and hydrogen (0.2 l min^{-1}) mixture using four cycles (each including 5 s of dosing followed by 15 min of hold time for diffusion). Finally, the reactor was heated to 1100 °C in pure argon atmosphere at 2 kPa (5 l min^{-1}) to melt the Cu and held for 5 min before the sample was cooled down with the reactor to room temperature naturally.

2.2. Graphene transfer

Graphene was transferred onto PITEM substrates using a polymethyl methacrylate (PMMA) carrier layer [40]. PMMA (4 wt% in anisole) was spin-coated on graphene at 1000 rpm for 15 s and 1500 rpm for 30 s, followed by drying in air for 2 min. The process was repeated three times to coat four-layers of PMMA on the graphene surface. Subsequently, the PMMA/graphene/metal stack was baked at 130 °C for 20 min. After cooling to room temperature, the metal foil was completely etched in 0.5 M $FeCl_3$ solution for 24 h and the obtained PMMA/graphene stack was floated on 3% HCl solution and DI water successively.

PITEM (hydrophobic, ~200 nm diameter track etched pores, ~8 μm thick) support (purchased from it4ip) was used as the transfer substrate. Prior to transfer, PITEM substrate was pre-treated with didecylamine (DDA, 0.05 M in ethanol) for 1 h to enhance its hydrophobicity, followed by 3 rinses (10 min each) in separate batches of ethanol to wash off any DDA residue. The PMMA/graphene stack floating on DI water was scooped onto the PITEM substrate, dried in air at room temperature and baked at 120 °C for 30 min to improve adhesion. Finally, acetone was used to remove the PMMA, followed by rinsing the graphene/PITEM in isopropanol and drying in air.

Graphene was also transfer onto 300 nm SiO_2/Si wafers using the PMMA method as detailed above [5–7, 9, 13, 20, 21, 23]. The only difference was once the PMMA/graphene stack was transferred onto a SiO_2 (300 nm)/Si wafer it was dried in air, followed by baking at 45 °C, 60 °C and 90 °C for 30 min each, washing in acetone overnight, and cleaning in IPA for 1 h.

The PMMA method was also used to transfer graphene to TEM grids [5–7, 9, 13, 20, 21, 23]. The PMMA/graphene stack was scooped from DI water using a copper TEM grid. The TEM grid with PMMA/graphene was baked in air at 60 °C for 30 min, and then placed in acetone hot vapours for 20 min, followed by washing in acetone overnight, cleaning in IPA, and drying in air.

2.3. Graphene characterization

SEM images of HSMG® graphene on Cu/Ni foils were acquired using FEI Helios NanoLab G3 CX scanning electron microscope at ~2 kV. SEM images of HSMG® graphene on PITEM membranes were collected by using a Zeiss Merlin Scanning Electron Microscope with Gemini II Column operated at ~2 kV.

The surface morphology of HSMG® graphene on growth substrate (Cu-Ni) was evaluated by a confocal laser scanning microscope (CLSM, Nikon MA200 microscope with inverted optics, equipped with a C1 confocal system) using an argon laser with a wavelength of $\lambda = 488$ nm. Images with resolution of 512×512 pixels were recorded using an EZ-C1 Free Viewer software, while detailed analysis of confocal microscopy data was performed using a Mountains Map Premium software (Digital Surf, France).

Raman spectra were obtained by using a Thermo Scientific DXR Confocal Raman spectrometer (~532 nm laser) with 1 mW laser power.

High-resolution transmission electron microscopy (HR-TEM) images were recorded by using an FEI Talos F200X transmission electron microscope.

2.4. Transport measurements

The pressure-driven ethanol transport and diffusion-driven solute transport measurements across the membranes were performed as reported elsewhere [2, 5–7, 9, 13, 20, 21, 23, 24, 41, 42]. A side-bi-side glass diffusion cell (figure 3(E), 7 ml volume on each side, 5 mm orifice, PermeGear, Inc.) with a gastight syringe (250 μl) installed on the short opening of the feed-side cell (left cell) was used for probing the transport of analytes through the membranes. The membrane was installed between two diffusion cells with the graphene side facing the feed side. Magnetic Teflon-coated stir bars were stirred vigorously at 1500 rpm in both cells to prevent concentration polarization. All the measurements were repeated for three times to obtain average values and standard deviations.

Initially, the system was washed three times (5 min each time) with ethanol (190 proof) to fully wet the membrane. Subsequently, ethanol was filled into both cells and a height difference in ethanol between feed and permeate side was generated to induce a hydrostatic pressure gradient. A digital camera was used to record the drop of ethanol meniscus level along the graduated syringe every 1 min. Ethanol permeance was calculated by $\text{permeance} = \frac{\Delta V}{\Delta P \times \Delta t \times \Delta A_{effective}}$, where ΔV is the ethanol volume change (drop), ΔP is the pressure difference across the membrane (~300–450 Pa), Δt is the time interval, and $A_{effective}$ is the effective membrane area during the transport process. Normalized flux was calculated by computing the ratio of ethanol permeance for PITEM +graphene membrane with respect to bare PITEM membrane.

Before performing diffusion-driven transport, the system was washed with DI water for five times to completely replace and remove ethanol. Four model solutes were selected for the transport measurements: KCl (hydrated diameter of K^+ ion ~0.662 nm, hydrated diameter of Cl^- ion ~0.664 nm), NaCl (hydrated diameter of Na^+ ion ~0.716 nm), Vitamin B12 (B12, molecular diameter ~1–1.5 nm), and Lysozyme (Lz, molecular diameter ~3.8–4 nm). For salt transport measurement (KCl or NaCl), the feed-side cell was filled with 7 ml of 0.5 M salt solution, while the permeate side was filled with 7 ml of DI water. A conductivity meter probe (connected to a Mettler Toledo SevenCompact S230 conductivity benchtop meter) immersed in the permeate side was used to measure the conductivity every 15 s for 15 min. For organic molecule transport measurements (B12 or Lz), the feed-side cell was filled with 7 ml of organic molecule solution (1 mM in 0.5 M KCl), while the right cell was filled with 7 ml of KCl solution (0.5 M). A fiber optic dip probe (attached to an Agilent Cary 60 UV–vis Spectrophotometer) immersed in the permeate side was used to record the absorbance spectra in the range of 190 to 1100 nm every 15 s for 40 min. The UV–vis intensity differences between B12 (peak position ~360 nm), Lz (peak position ~282 nm) and DI water (reference wavelength ~710 nm) were used for computing the concentration of permeating species.

The transport rate of each solute was calculated via the slope of concentration change in the permeate side, and the normalized flux was computed by computing the ratio of transport rate for PITEM+graphene membrane with respect to bare PITEM substrate. The effective normalized flux was calculated by $\left(\frac{\textit{normalized flux of each species} - \textit{normalized flux of ethanol}}{1 - \textit{normalized flux of ethanol}}\right)$.

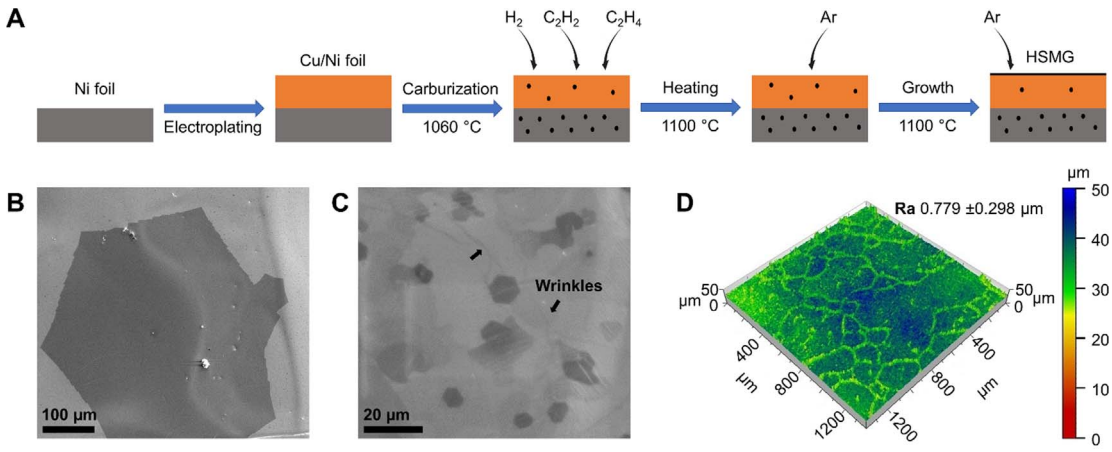

Figure 1. (A) Schematic of the High Strength Metallurgical Graphene (HSMG®) synthesis process. (B), (C) SEM images of HSMG® on growth substrate (Cu/Ni foil). (D) Confocal Laser Scanning Microscopy (CLSM) image of HSMG® on growth substrate (Cu/Ni foil).

3. Results and discussion

3.1. Characterization of graphene synthesized on liquid Cu

Large-area graphene was synthesized on a liquid Cu via the HSMG® process [35, 38, 39] with some modifications (figure 1(A)). Pre-carburized Ni foil was used as a support for electroplating Cu due to the higher melting point of Ni and good wettability of nickel by Cu. The bimetal was heated in a chamber and carburized in hydrocarbon vapors without forming any carbon deposits on the Cu surface. Next, the Cu is molten by increasing the temperature and the lower carbon solubility in liquid Cu than solid Cu pushes carbon to the top of the Cu surface, resulting in the formation of monolayer graphene [31, 35, 39, 43]. The main advantage of this method is the potential for self-assembly for the growing graphene domains (high mobility and/or rotation on the liquid Cu surface) minimizing defects along domain boundaries in a continuous monolayer film [31]. SEM image in figure 1(B) shows large graphene domains (~500 μm) due to low graphene nucleation density and faster growth rates at high temperature (>1080 °C) [29–35]. Figure 1(C) shows a continuous film of graphene covering the catalyst surface identified via wrinkles like features in graphene that arise from differences in thermal expansion between graphene and Cu during cooling process in HSMG®. Some small areas of multi-layer graphene regions (darker contrast) resulting from excess carbon supply during synthesis are also seen.

The surface morphology of HSMG® graphene on growth substrate (CLSM image in figure 1(D)) shows visible Cu grains of various sizes with a surface roughness Ra ~ 0.779 ±0.298 μm. We note that the surface roughness results from the slow heteroepitaxial growth of solid Cu grains on the nickel substrate [44].

To assess the quality of HSMG®, we acquired HR-TEM images as well as Raman spectra (figure 2). HR-TEM images (figure 2(A)) show a film with some line like features. Magnified regions in the center, left, and right side of the feature are marked with red, green, and purple boxes, respectively. Figure 2(B) shows a high degree of defects along the line like feature, consistent with prior observations of defect clusters along graphene domain boundaries in HSMG® [31]. Figures 2(C) and (D) present atomic resolution images of the graphene lattice from two different regions. Notably, figure 2(C) shows several atoms missing (indicated by green arrows), while figure 2(D) appears to be pristine with no apparent vacancies being readily visible. Figure 2(E) also presents an HR-TEM image of graphene with visible multilayers and wrinkles, which is consistent with SEM images in figure 1(C).

Upon transferring HSMG® graphene onto SiO_2/Si substrate (figure 2(F)), Raman spectra also confirm the presence of monolayer graphene (I_{2D}/I_G ~2, full width at half-maximum (FWHM) of 2D peak ~33.5, I_D/I_G ~0.09), multilayer graphene patches (I_{2D}/I_G <1, FWHM of 2D peak ~54.4, I_D/I_G ~0.04) and wrinkles (I_D/I_G ~0.36) [45, 46]. The D peak and increased I_D/I_G ratio indicate the presence of defects associated with graphene wrinkles. We note that the I_D/I_G ratio of monolayer HSMG® ~0.09 is higher than that of high-quality CVD graphene [20] ~0.027, further confirming higher intrinsic defect density in HSMG®.

3.2. Graphene transfer onto PITEM substrate and fabrication of atomically thin membranes

The synthesized HSMG® graphene was transferred onto PITEM substrate using a sacrificial polymer (figure 3(A), see Methods section) to form an atomically thin membrane. We specifically choose PITEM with parallel cylindrical pores ~200 nm diameter as model supports due to (i) its straight, well-defined channels that effectively prevent inter-connected pores and allow for unambiguous interpretation of transport measurements

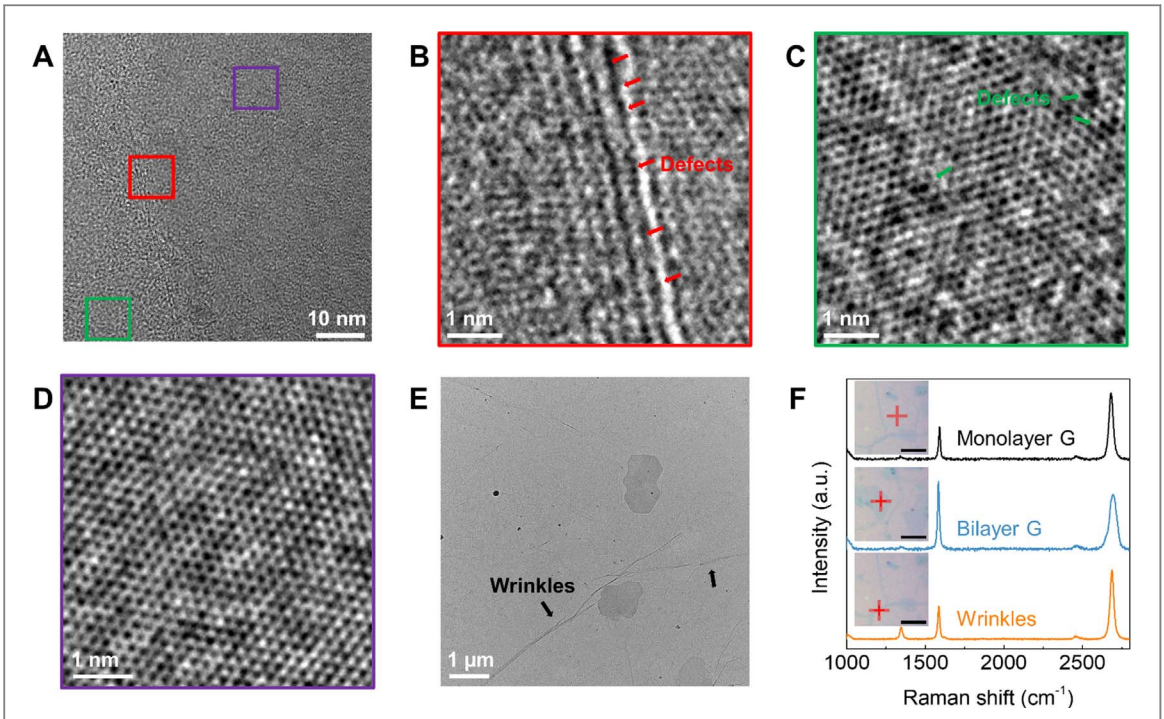

Figure 2. (A) Transmission electron microscopy (HRTEM) image of HSMG®, with magnified regions in the center, left, and right side of the line like feature marked with red, green, and purple boxes, respectively. (B) HR-TEM image of line like feature with defects (red arrows along the feature). (C) Atomic resolution image of the graphene lattice with defects (several atoms missing indicated by green arrows). (D) Atomic resolution image of pristine graphene lattice region with no readily apparent vacancies. (E) TEM image of monolayer HSMG® graphene film with some multilayer islands/domains and wrinkles. (F) Raman spectra of HSMG® graphene transferred onto SiO_2/Si probed over three distinct regions i.e. monolayer, multilayer, and wrinkles (insets show corresponding optical images, scale bars are 10 μm).

and (ii) PITEM's compatibility with acetone, which has to be used to dissolve polymer carrier layer from transfer.

SEM images (figures 3(B), (C) confirm successful transfer of HSMG® onto PITEM support, where most PITEM pores are covered with graphene and appear darker due to graphene's electrical conductivity (figures 3(B), (C)). Uncovered PITEM pores appear brighter due to polymer charging [5, 20]. Wrinkles in graphene are also observed in the SEM images as well as some tears in graphene that appear as bright open regions co-located along wrinkles in some instances (figure 3(B)). To further confirm the transfer of HSMG® onto PITEM support, we collected the Raman spectra on bare PITEM and HSMG® transferred onto PITEM (PITEM+HSMG®). As shown in the figure 3(D), compared with bare PITEM, there is a clear 2D peak which belongs to HSMG® in the PITEM+HSMG® sample (G peak is overlapped with the Raman signal of PITEM), indicating the successful transfer of HSMG® onto PITEM.

3.3. Assessing the quality of graphene via ionic and molecular transport

The synthesized atomically thin monolayer graphene membrane was mounted in a side-bi-side diffusion cell (figure 3(E)) to evaluate the nanometer and sub-nanometer scale defects over large area by measuring pressure-driven ethanol transport and diffusion-driven transport of salts/organic molecules. The pressure-driven transport of ethanol was performed to assess the tears and large nanopores (>60 nm), since the pressure-driven flow through a PITEM pore and a graphene pore scales as D^4_{PITEM}/L_{PITEM} and $D^3_{graphene}$, respectively [20, 24], i.e. ~60 nm defect in graphene will have similar resistance to transport as an open PITEM ~200 nm pore. Diffusion-driven flow on the other hand through a PITEM pore and a graphene pore scales as scales a D^2_{PITEM}/L_{PITEM} and $D^1_{graphene}$, respectively, i.e. ~4 nm defect in graphene will have similar resistance to transport as an open PITEM ~200 nm pore. Hence, diffusion is sensitive to nanoscale defects in graphene <4 nm and diffusion-driven transports of KCl, NaCl, B12 and Lz were performed to evaluate the sub-nanometer defects as well as small nanopores ($\leqslant$4 nm) [2, 5–7, 9, 13, 20, 21, 23, 24, 41, 42].

The normalized flux of ethanol through PITEM+HSMG® with respect to bare PITEM is ~6.7%, indicating a high-yield graphene transfer ~93.3%. This value is comparable with most prior results using CVD graphene [20, 23, 24, 40, 47–49], but slightly lower than CVD graphene transferred via isopropanol-assisted hot lamination (IHL) method (figure 3(F)) [20]. We note that the percentage of multi-layer graphene in the total area of representative HSMG® is ~30% (figure 1(C)), which is higher than that of high-quality CVD graphene ~3%

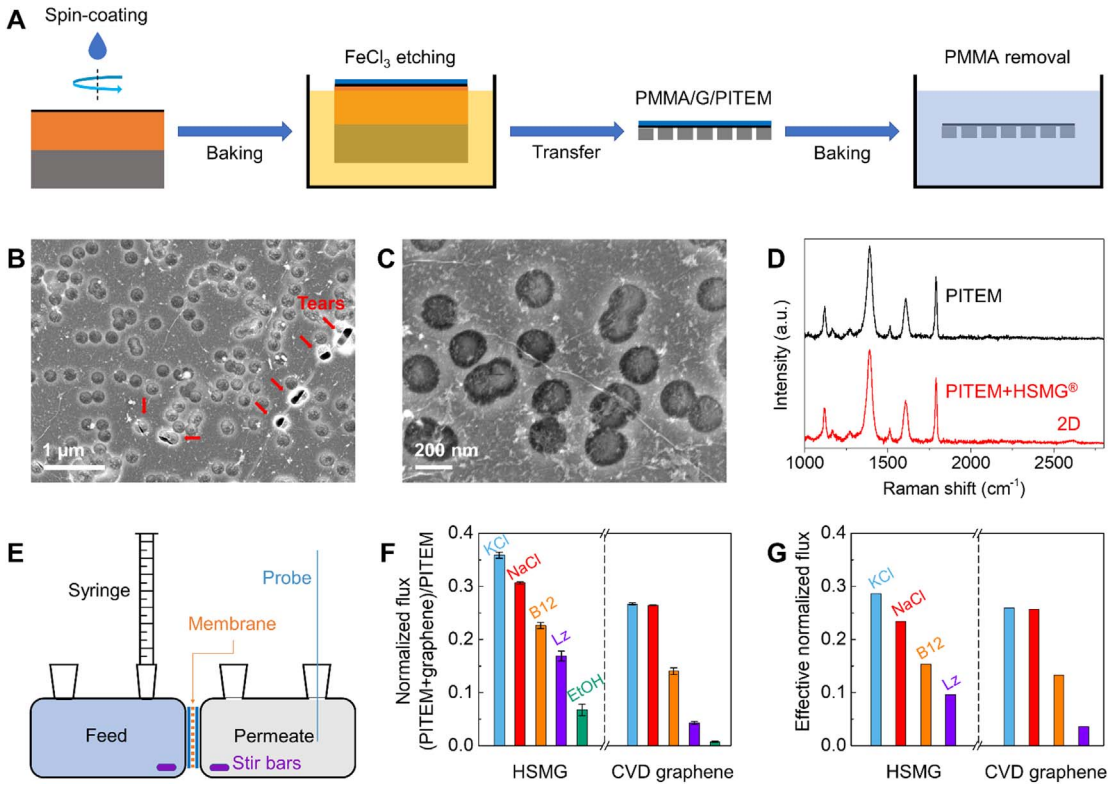

Figure 3. (A) Sacrificial polymer scaffold method used to transfer HSMG® graphene onto polyimide track etched (PITEM) support. (B) and (C) SEM images of HSMG® transferred onto PITEM supports. Red arrows indicate tears. Wrinkles in the graphene are also visible. (D) Raman spectra of PITEM substrate (black curve) and HSMG® transferred onto PITEM (PITEM+HSMG®, red curve). (E) Schematic of customized side-bi-side diffusion cell. (F) Normalized flux of HSMG® and high-quality CVD graphene grown on solid Cu [20] for pressure-driven ethanol flow and diffusion-driven flow of KCl, NaCl, B12, and Lz. The normalized flux was computed by the flow rate of PITEM+HSMG® membrane divided by that of the bare PITEM substrate. (G) Effective normalized flux of HSMG® graphene and high-quality CVD graphene [20] after accounting for coverage.

[20]. The multi-layer percentage is important for transport measurements since multi-layer graphene is expected to show a higher resistance against the solute transport than monolayer graphene. Diffusion-driven transport of KCl (~0.66 nm), NaCl (~0.716 nm), Vitamin B12 (~1–1.5 nm), and Lysozyme (Lz) (~3.8–4 nm) through HSMG® show normalized fluxes ~35.8%, ~30.6%, ~22.6%, and ~16.9%, respectively. On the other hand, high-quality CVD graphene transferred via IHL shows the normalized flux of KCl ~26.7%, NaCl ~26.4%, B12 ~14%, and Lz ~4.3%, respectively [20].

Since HSMG® shows higher transport of hydrated ions and organic molecules than high-quality CVD graphene (transferred via IHL), this implies more sub-nanometer and nanometer scale defects existing in HSMG®. However, the transfer yields are also different. The effective normalized flux computed using the equation $\left(\frac{normalized\ flux\ of\ each\ species\ -\ normalized\ flux\ of\ ethanol}{1\ -\ normalized\ flux\ of\ ethanol}\right)$ facilitates a direct comparison and allows for accounting for any un-transferred areas that would be akin to bare PITEM (figure 3(G)) and can be effectively subtracted out. Compared with high-quality CVD graphene transferred via IHL method (KCl~26%, NaCl~25.7%, B12 ~13.3%, and Lz ~3.6%) [20] (figure 3(G)), HSMG® shows similar/comparable effective normalized flux of KCl ~28.6%, NaCl ~23.4%, and B12 ~15.4%, but much higher effective normalized flux of Lz ~9.6%, indicating that HSMG® lattice has more defects >4 nm.

The high quality of the HSMG® graphene is attributed to the high-temperature of synthesis and large graphene domains formed which are highly mobile on the smooth/flat liquid Cu surface, [31, 50], while defects >4 nm could potentially also result from re-crystallization of liquid Cu and associated mechanical stress on the graphene. The presence of intrinsic defects in HSMG® graphene at similar levels as on solid Cu (optimized for membrane applications) indicates the formation of intrinsic defects within the graphene domains during bottom-up synthesis. The synthesis of graphene on liquid Cu also does not eliminate the problem of the wrinkles formation, which is mainly due to the different thermal expansion coefficients of graphene and Cu [51]. Notably, solidification of the graphene growth substrate changes the morphology of the Cu surface from perfectly smooth in the liquid state (during graphene growth) to grainy in the solid state (before graphene transfer to PITEM) and the graphene adapts to these changes via elastic stretching. Taken together, the quality of

HSMG® is comparable with high-quality CVD graphene grown on solid Cu and optimized for membrane applications.

4. Conclusions

In this work, the quality of large-area graphene synthesized on liquid copper for membrane applications was investigated. Graphene (HSMG®) was synthesized using the metallurgical method and assessed via a simple and cost-effective technique based on pressure-driven and diffusion-driven transport of analytes. The as-synthesized HSMG® showed a high-yield transfer onto PITEM with >93% coverage, but intrinsic sub-nanometer and nanometer scale defects still exist in HSMG® and are no less than high quality CVD graphene synthesized on solid Cu and optimized for membrane applications. Even though HSMG® graphene is synthesized at high-temperature and has large hexagonal domains, with potential for self-assembly via high mobility on the smooth/flat liquid surface, intrinsic sub-nanometer and nanometer-scale defects are inevitably present as reflected in the evidenced transport of analytes (0.66–4 nm). Our study effectively benchmarks quality of graphene grown on liquid copper for membrane applications and also provides fundamental insights into the origin of intrinsic defects in large-area graphene synthesized via bottom-up processes for membrane applications.

Acknowledgments

This work was supported in part by NSF CAREER #1944134, in part by DOE grant # DESC0022237, and in part by DOE Early Career Award # DE-SC0022915 to P.R.K. G.R. would like to acknowledge 'Implementation Doctoral School' project no. POWR.03.02.00–00-I042/16–00, Dean of Mechanical Faculty of Lodz University of Technology, Dean of Mechanical Faculty and Vice-Rector for Science of Lodz University of Technology for financial support. The authors would like to thank Radomir Atraszkiewicz and Adam Rzepkowski for the HSMG® graphene synthesis processes, and Witold Szymański for conducting morphology measurements.

Data availability statement

All data that support the findings of this study are included within the article (and any supplementary files).

ORCID iDs

Grzegorz Romaniak https://orcid.org/0000-0001-7711-1540
Peifu Cheng https://orcid.org/0000-0001-6010-6411
Konrad Dybowski https://orcid.org/0000-0003-4017-3830
Piotr Kula https://orcid.org/0000-0002-1796-9155
Piran R Kidambi https://orcid.org/0000-0003-1546-5014

References

[1] Yang Y *et al* 2019 Large-area graphene-nanomesh/ carbon-nanotube hybrid membranes for ionic and molecular nanofiltration *Science* **364** 6445
[2] O'Hern S C *et al* 2015 Nanofiltration across defect-sealed nanoporous monolayer graphene *Nano Lett.* **15** 3254–60
[3] Jang D, Idrobo J C, Laoui T and Karnik R 2017 Water and solute transport governed by tunable pore size distributions in nanoporous graphene membranes *ACS Nano.* **11** 10042–52
[4] Surwade S P *et al* 2015 Water desalination using nanoporous single-layer graphene *Nat. Nanotechnol.* **10** 459–64
[5] Cheng P *et al* 2020 Facile size-selective defect sealing in large-area atomically thin graphene membranes for sub-nanometer scale separations *Nano Lett.* **20** 5951–9
[6] Kidambi P R *et al* 2017 Nanoporous atomically thin graphene membranes for desalting and dialysis applications *Adv. Mater.* **29** 1700277
[7] Kidambi P R *et al* 2018 Facile fabrication of large-area atomically thin membranes by direct synthesis of graphene with nanoscale porosity *Adv. Mater.* **30** 1804977
[8] Jain T *et al* 2015 Heterogeneous sub-continuum ionic transport in statistically isolated graphene nanopores *Nat. Nanotechnol.* **10** 1053–7
[9] Cheng P *et al* 2022 Differences in water and vapor transport through angstrom-scale pores in atomically thin membranes *Nat. Commun.* **13** 6709
[10] Chaturvedi P, Moehring N K, Cheng P, Vlassiouk I, Boutilier M S H and Kidambi P R 2022 Deconstructing proton transport through atomically thin monolayer CVD graphene membranes *J. Mater. Chem.*A **10** 19797–810
[11] Hu S *et al* 2014 Proton transport through one-atom-thick crystals *Nature* **516** 7530
[12] Kidambi P R, Chaturvedi P and Moehring N K 2021 Subatomic species transport through atomically thin membranes: present and future applications *Science* **374** 6568

[13] Cheng P et al 2022 Nanoporous atomically thin graphene filters for nanoscale aerosols ACS Appl. Mater. Interfaces 14 41328–36
[14] Boutilier M S H, Jang D, Idrobo J C, Kidambi P R, Hadjiconstantinou N G and Karnik R 2017 Molecular sieving across centimeter-scale single-layer nanoporous graphene membranes ACS Nano. 11 5726–36
[15] Jiang D E, Cooper V R and Dai S 2009 Porous graphene as the ultimate membrane for gas separation Nano Lett. 9 4019–24
[16] Huang S et al 2018 Single-layer graphene membranes by crack-free transfer for gas mixture separation Nat. Commun. 9 2632
[17] Schneider G F et al 2010 DNA translocation through graphene nanopores Nano Lett. 10 3163–7
[18] Merchant C A et al 2010 DNA translocation through graphene nanopores Nano Lett. 10 2915–21
[19] Prozorovska L and Kidambi P R 2018 State-of-the-art and future prospects for atomically thin membranes from 2D materials Adv. Mater. 30 1801179
[20] Cheng P, Moehring N K, Idrobo J C, Ivanov I N and Kidambi P R 2021 Scalable synthesis of nanoporous atomically thin graphene membranes for dialysis and molecular separations: via facile isopropanol-assisted hot lamination Nanoscale. 13 2825–37
[21] Kidambi P R et al 2018 A scalable route to nanoporous large-area atomically thin graphene membranes by roll-to-roll chemical vapor deposition and polymer support casting ACS Appl. Mater. Interfaces 10 10369–78
[22] Wang L, Boutilier M S H, Kidambi P R, Jang D, Hadjiconstantinou N G and Karnik R 2017 Fundamental transport mechanisms, fabrication and potential applications of nanoporous atomically thin membranes Nat. Nanotechnol. 12 509–22
[23] Kidambi P R et al 2017 Assessment and control of the impermeability of graphene for atomically thin membranes and barriers Nanoscale. 9 8496–507
[24] Kidambi P R, Boutilier M S H, Wang L, Jang D, Kim J and Karnik R 2017 Selective nanoscale mass transport across atomically thin single crystalline graphene membranes Adv. Mater. 29 1605896
[25] Kula P et al 2016 High strength metallurgical graphene for hydrogen storage nanocomposites Vacuum 129 79–85
[26] Pawlak R, Lebioda M, Rymaszewski J, Szymanski W, Kolodziejczyk L and Kula P 2017 A fully transparent flexible sensor for cryogenic temperatures based on high strength metallurgical graphene Sensors 17 51
[27] Gajewski K et al 2016 Kelvin probe force microscopy investigations of high strength metallurgical graphene transferred on low-density polyethylene Microelectron. Eng. 157 71–7
[28] Kunikowska A et al 2020 High strength metallurgical graphene as an additional reinforcing phase for carbon fibre composites Archiv. Civ. Mech. Eng. 20 25
[29] Kim M S et al 2019 Comparison of growth behavior and electrical properties of graphene grown on solid and liquid copper by chemical vapor deposition J. Nanosci. Nanotechnol. 20 316–23
[30] Zheng S et al 2019 Insight into the rapid growth of graphene single crystals on liquid metal via chemical vapor deposition Sci China Mater. 62 1087–95
[31] Kuten D, Dybowski K, Atraszkiewicz R and Kula P 2020 Quasi-monocrystalline graphene crystallization on liquid copper matrix Materials. 13 2606
[32] Liu J and Fu L 2019 Controllable growth of graphene on liquid surfaces Adv. Mater. 31 1800690
[33] Geng D et al 2012 Uniform hexagonal graphene flakes and films grown on liquid copper surface Proc. Natl. Acad. Sci. USA 109 7992–6
[34] Ding G et al 2013 Chemical vapor deposition of graphene on liquid metal catalysts Carbon N Y. 53 321–6
[35] Kula P et al 2014 Single and multilayer growth of graphene from the liquid phase Applied Mechanics and Materials. 510 8–12
[36] Wang L, Ding Y, Wang X, Lai R, Zeng M and Fu L 2021 In situ investigation of the motion behavior of graphene on liquid copper Adv. Sci. 8 2100334
[37] Moehring N K et al 2022 Kinetic control of angstrom-scale porosity in 2D lattices for direct scalable synthesis of atomically thin proton exchange membranes ACS Nano. 16 16003–18
[38] Kula P, Rzepkowski A, Pietrasik R, Atraszkiewicz R, Dybowski K and Modrzyk W 2016 Method of producing graphene from liquid metal U.S. Patent 9284640B2
[39] Kula P et al 2015 High strength metallurgical graphene—mechanisms of growth and properties Arch. Metall. Mater. 4 2535–41
[40] Cheng C, Iyengar S A and Karnik R 2021 Molecular size-dependent subcontinuum solvent permeation and ultrafast nanofiltration across nanoporous graphene membranes Nat. Nanotechnol. 16 989–95
[41] O'Hern S C et al 2014 Selective ionic transport through tunable subnanometer pores in single-layer graphene membranes Nano Lett. 14 1234–41
[42] O'Hern S C et al 2012 Selective molecular transport through intrinsic defects in a single layer of CVD graphene ACS Nano. 6 10130–8
[43] Kolodziejczyk L, Kula P, SzymaDski W, Atraszkiewicz R, Dybowski K and Pietrasik R 2016 Frictional behaviour of polycrystalline graphene grown on liquid metallic matrix Tribol. Int. 93 628–39
[44] Tammann G and Swenson L G 1925 A Text Book of Metallography Translated From The Third German Edition ed R S Dean and L G Swenson (The Chemical Catalog) (New York, Journal of the Society of Chemical Industry) 1925, p 388
[45] Ferrari A C and Basko D M 2013 Raman spectroscopy as a versatile tool for studying the properties of graphene Nat. Nanotechnol. 8 235–46
[46] Calizo I, Bejenari I, Rahman M, Liu G and Balandin A A 2009 Ultraviolet Raman microscopy of single and multilayer graphene J. Appl. Phys. 106 043509
[47] Shen L et al 2021 Highly porous nanofiber-supported monolayer graphene membranes for ultrafast organic solvent nanofiltration Sci. Adv. 7 eabg6263
[48] Suk J W et al 2011 Transfer of CVD-grown monolayer graphene onto arbitrary substrates ACS Nano. 5 6916–24
[49] Wittmann S et al 2023 Assessment of wafer-level transfer techniques of graphene with respect to semiconductor industry requirements Adv. Mater. Technol. 8 2201587
[50] Geng D et al 2014 Self-aligned single-crystal graphene grains Adv. Funct. Mater. 24 1664–70
[51] Amini S, Garay J, Liu G, Balandin A A and Abbaschian R 2010 Growth of large-area graphene films from metal-carbon melts J. Appl. Phys. 108 094321